Dislocations and Related Defects in Niobium Oxide Structures
Author(s): J.S. Anderson, J.L. Hutchison and F.J. Lincoln
Source: *Proceedings of the Royal Society of London. Series A, Mathematical and Physical Sciences*, Vol. 352, No. 1670 (Jan. 7, 1977), pp. 303-323
Published by: The Royal Society
Stable URL: http://www.jstor.org/stable/79218
Accessed: 03/05/2014 23:05

Proc. R. Soc. Lond. A. **352**, 303–323 (1977)
Printed in Great Britain

Dislocations and related defects in niobium oxide structures

By J. S. Anderson, F.R.S.,† J. L. Hutchison† and F. J. Lincoln‡
Inorganic Chemistry Laboratory, University of Oxford

(*Received* 20 *August* 1975)

[Plates 1 and 2]

Lattice images of the niobium oxides, structures based on the linkage of octahedral groups in continuous networks, occasionally contain features recognizable as dislocations. Since lattice imaging enables the microstructure to be resolved in great detail, at the level of local structural organization, it is possible to determine the configuration, and also to infer the chemical composition, of dislocated areas. By treating the niobium oxide 'block' structures as superstructures of the ReO_3 (DO_9) type, the topology of dislocations can be expressed by relations between the insertion (or deletion) of one or more half-planes of cations, or of oxygen atoms only, changes in the number of crystallographic shear plane interfaces between blocks or columns, changes in (idealized) dimensions and any requisite distortion in the third dimension. Mapping the structure around a dislocation, from the lattice image, is directly equivalent to plotting the Burgers' circuit.

In this way, the precise nature of a dislocating perturbation and its implications for the local chemical composition of the crystal can be directly identified. The method is exemplified by analysis of dislocations and of related extended defects of several types, associated with twinning phenomena, semicoherent intergrowth between different ReO_3-type superstructures and arrays building up a low angle boundary. The essential features of the analysis are not restricted to structures of the niobium oxide type, but can be extended to other types of polyhedron networks.

Introduction

Direct lattice imaging methods of electron microscopy have given a new insight into crystallography in real space, in that they have made it possible to detect and identify extended defects or local fluctuations in structure and composition. In crystals based on the more open structural types it is virtually possible to resolve, in projection, the positions of the heavy atoms (see, for example, Iijima 1971, 1973; Allpress & Iijima 1973; Browne & Anderson 1974), thereby identifying the local structure, as distinct from the averaged defect structure, with certainty.

† Present address: Edward Davies Chemical Laboratory, University College of Wales, Aberystwyth SY23 1NE.
‡ Permanent address: University of Western Australia, Nedlands, W. A.

This development has hitherto been applied largely to the study of fluctuations or variability of composition, to local modifications of superstructure ordering and related problems. It is, however, possible to examine in detail other types of extended defect, and this paper discusses dislocations and related defects in 'block' structure crystals, of the niobium oxide type, as analysed from lattice images.

These 'block' structures combine a remarkable flexibility of superstructure ordering, to accommodate changes of chemical composition (Wadsley & Andersson 1970) with strict topological constraints. Their structural principle is the linkage of octahedral [MO_6] groups, which share apices to build up an open framework as in ReO_3. This sub-structure is collapsed by the operation of two sets of crystallographic shear planes (c.s. planes), which create walls of edge-sharing octahedra

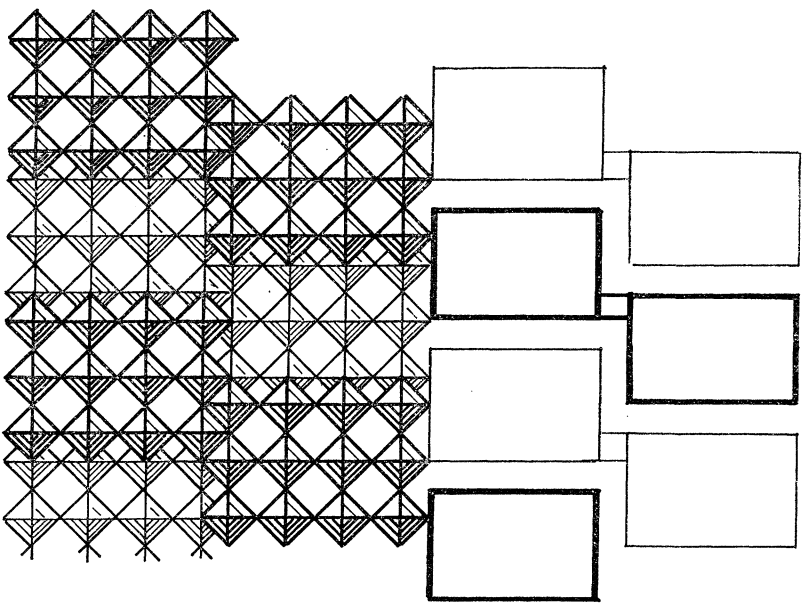

FIGURE 1. Structure of monoclinic $Nb_{12}O_{29}$: columns (4×3) octahedra linked in ribbons. Right hand side: schematic representation, with rectangles delineating the peripheral cation sites.

and divide the whole into two sets of rectangular columns, each of which has essentially the ReO_3 structure, as exemplified by $Nb_{12}O_{29}$ (figure 1). Across such an interface between columns, the cations are necessarily displaced by one half the octahedron diagonal in order that their octahedral groups may share a common edge. Within this topological pattern, considerable variation in the total anion: cation ratio can be accommodated by changes in either the orientation or the spacing of regularly recurrent c.s. planes (in perfect structures), or by localized, space-filling variations in the cross-sections of the ReO_3-like columns (in faulted structures).

Although the octahedral groups are not strictly regular, little error is introduced by regarding each column as having the idealized ReO_3 structure, with the cations located on a cubic mesh of 0.39 nm side. In general, all local faulted structures can be completely mapped on that basis, without any misfit. However, Iijima (1973) inferred from one lattice image of a disordered crystal of H-Nb_2O_5 that a dislocation was included within the field mapped, and we have, from time to time, also found dislocations in the course of extensive work in this laboratory. In every case these have been grown-in dislocations, not artefacts produced during the fracture of crystals for electron microscopic examination. They occur rarely in the thin crystal flakes used for lattice imaging and can be neither produced nor found at will. In several cases it has been possible to elucidate the structures right up to, or into, the core of the dislocations, and thence to derive a rather detailed insight into them. We discuss here some general principles governing dislocations in these, at first sight, rather complex structures and analyse a few dislocations and related faults – e.g. incoherent boundaries – that have been encountered.

General principles of dislocations in niobium oxide structures

We consider first the structural implications of introducing one or more additional half planes of atoms into the crystals – i.e. a pure edge dislocation or the edge component of a mixed dislocation, as seen in projection. Edge dislocations in ionic crystals inherently introduce complexities that are absent from dislocations in elementary crystals, since the introduction of an extra half-plane of atoms into one sublattice necessarily alters the stoichiometry of the crystal. If one constituent (usually the cation) can adopt more than one valence state, this defect of stoichiometry may be tolerated. For example, in the niobium oxides, insertion of a half-plane of cations or abstraction of a half-plane of oxygen can be balanced by a corresponding conversion of niobium(v) cations to the niobium(iv) valence state. In addition, these and other polyhedron network structures present some special features. The virtual unit of structure is the cation coordination polyhedron – in this case the $[MO_6]$ octahedral group – rather than the atomic cation or anion; all the microstructural evidence supports the view that octahedral coordination, and the linkage of the octahedral groups by vertex-sharing or edge sharing, are conserved as strictly as possible in defect structures. A topological constraint is thereby placed upon the structure around a dislocation. Within this pattern, superstructure ordering is flexible enough to allow some reorganization of vertex and edge sharing between octahedra, and of shifts in the interfaces between columns. Subtle changes of composition can thereby be incorporated in extended defects. One consequence of this is that, for certain displacements that introduce a slice or wedge of new structure into a crystal, and that could be formally described as resulting from a displacement operating upon the original structure, any elastic deformation can be eliminated, to a first approximation, by a local rearrangement of column interfaces. For

idealized structures, the elimination of strain would be complete; in the real structures, the octahedral groups are not strictly regular and residual atomic displacements may well remain.

In all these structures, one cell dimension is short (one octahedron diagonal); the other two axes are long, and any displacement involving a unit vector of the structure as a whole would be improbably large. However, all are superstructures on the ReO_3 motif, and the relevant displacement vectors can be unit vectors of the small, simple cubic sub-cell. These, operating on the superstructure, can generate variant configurations that are consistent with the topology of the 'block' structures.

Within any crystal of this type, the characteristic dimensions of any region can be specified by considering a file of columns, enclosed between adjacent c.s. planes and extending along some main direction of the superstructure, as is shown by hatching in figure 3*a*. Any one column, with cross section $l_a \times l_c$ octahedra, as measured along the *a* and *c* directions of the sub-cell, contributes l rows containing cations (with the composition MO_2) and $l-1$ rows containing only oxide ions to the length of some finite strip within the file. In an idealized structure, successive rows of both kinds are regularly spaced at a modular distance (*ca.* 0.2 nm) along the sub-cell axes. In an unfaulted, stoichiometric crystal, all the columns within the file would be either identical (as in $Nb_{12}O_{29}$) or of regularly alternating size (as in H–Nb_2O_5). In a real crystal, with defects of order and composition, this is not necessarily the case, as has clearly emerged from the electron microscopy. Quite generally, within a finite strip embracing N columns, let there be n_i, n_j... columns with the dimensions l_i, l_j... along the direction considered. Then $N = \sum_i n_i$, and the total numbers of cation rows ($= n_{Nb}$) and oxygen-only rows ($= n_O$) are

$$n_{Nb} = \sum_i n_i l_i \quad \text{and} \quad n_O = \sum_i n_i (l_i - 1) = n_{Nb} - N.$$

The total length w contributed to the file by the strip of N columns is

$$w = \sum_i n_i (2l_i - 1) = 2n_{Nb} - N,$$

expressed in modular units of the semi-octahedron diagonal.

An edge dislocation parallel to the unique crystallographic axis may involve inserting (or removing) one or more half-sheets of atoms, seen in projection as a cation row, an anion row or both. Because of the topological constraint, a half-sheet of cations can be inserted (or a half-sheet of oxide ions removed) only by forming an additional wall of edge-sharing octahedra; conversely, insertion of a half-sheet of oxide ions (or removal of a half-sheet of cations) necessarily converts edge-sharing octahedra to vertex-sharing octahedra. The c.s. plane interfaces between columns are thus rearranged and the number of columns included within the strip will thereby be changed; the cross-sections of the columns will be altered. For changes Δn_{Nb}, Δn_O, ΔN in the numbers of atom rows and columns,

$$\Delta n_O = \Delta n_{Nb} - \Delta N$$

and the idealized length of the finite strip is altered by

$$\Delta w = 2\Delta n_{\mathrm{Nb}} - \Delta N.$$

In so far as dimensional changes have to be compensated by local elastic deformation, it is likely that in most cases, for any one dislocation, $\Delta w \leqslant 2$ (i.e. $\Delta w \leqslant a_{\mathrm{R}}$), larger displacements being split up into separated partials.

Table 1 summarizes the consequences of inserting or deleting cation rows or oxide ion rows, for cases with a total dimensional change $\Delta w \leqslant a_{\mathrm{R}}$. It provides a basis for analysing dislocations and extended defects in structures, as mapped from lattice images. Entries 1 and 2, involving no change in dimensions, are not

TABLE 1. ALTERATIONS IN DIMENSIONS AND IN NUMBERS OF C.S. INTERFACES DUE TO INSERTION OF EXTRA HALF-PLANES OF CATIONS OR ANIONS

	Δw	Δn_{Nb}	Δn_{O}	ΔN
1	0	0	0	0
2		± 1	∓ 1	± 2
3	± 1	± 1	0	± 1
4		0	± 1	∓ 1
5	± 2	± 1	± 1	0
6		± 2	0	± 2
7		0	± 2	∓ 2

trivial. By 1 is implied the effect of transferring one complete row of octahedra from one column to another; there is no change in n_{Nb} or n_{O}, but the c.s. interface between columns is moved one step. This is a basic step in diffusion and reaction processes (Browne & Anderson 1974) and local perturbations of the basic structure are often accommodated in this way. The size and connectivity of columns can thereby adjust themselves, without change of composition, in the neighbourhood of extended defects. In 2, a cation row is deleted and an oxide ion row inserted (or vice versa), so that there is no net dimensional change but, necessarily, a change in column cross-sections and connectivity. The composition of the crystal is changed, and the defect may be exemplified by the structural changes involved in the segregation of impurity atoms bearing a different formal charge (Anderson, Browne & Hutchison 1972*a*).

Entries 3 and 4 in table 1 can be regarded as the primary unit edge dislocations. Larger dislocations, such as 5–7, may frequently involve closely spaced partials of type 3 and 4. It may be noted that if 3 and 4 operate successively upon the structure, but in opposite senses, they will generate a closed domain of distorted structure within a dimensionally consistent crystal. Outside this strained region, their net effect is equivalent to the situation 2, defined above, and 2 corresponds to the case where the (respectively positive and negative) partials 3 and 4 are coterminous.

The foregoing relates to the projection of the structure down the unique short (0.4 nm) axis which, as discussed below, can be interpreted from the lattice image.

We next consider the implications for a real, three dimensional crystal. As was emphasized earlier, the cations on either side of a c.s. interface are necessarily separated in height by $\frac{1}{2}a_{\mathrm{R}}[010]$ in order that their octahedral groups may share edges. It has been seen that the insertion or deletion of a half-plane of atoms implies a change of ± 1 in the number of c.s. interfaces. As a consequence, the original regular alternation of levels in traversing any Burgers' circuit would be destroyed. Nevertheless, the topological requirements for linkage of octahedral

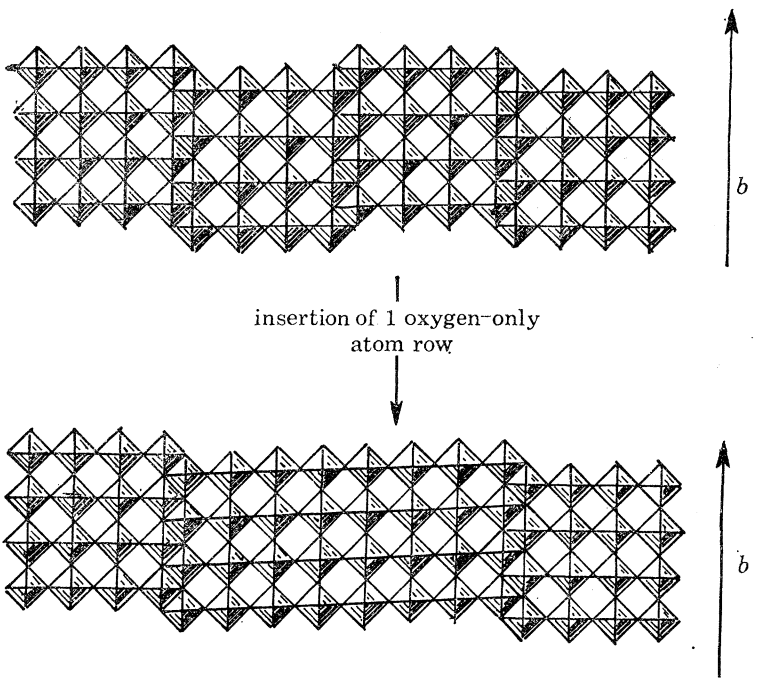

FIGURE 2. Change of ± 1 in number of column interfaces involves canting the cation layers to satisfy the topological constraint.

groups must be satisfied, and this can be done only if there is a distortion along the [010] direction. As is shown in figure 2, the requisite mating of octahedra can be achieved only if the sheets of cations are tilted with respect to the $(010)_{\mathrm{R}}$ planes of the idealized structure. Iijima recognized this 'canting' of columns in the dislocation that he identified. It is a necessary structural consequence of the change in the number of c.s. interfaces, provided that ΔN is odd; if ΔN is even, mapping around a Burgers' circuit does not produce an apparent mismatch of cation levels. In figure 2 and the schematic Burgers' circuits of figure 3, this consequential tilting is represented as localized at the closure gap. In the real crystal it will be distributed as a progressively attenuated warping of lattice planes, by small relaxations of all atomic positions.

Having so defined the components of dimensional distortion along the sub-cell axes, we next consider the relation between the distorted structure and its lattice

image. This displays (*a*) the cross sections of the individual columns and (*b*) their connectivity. The modular dimensions of an idealized structure enable this information to be translated directly into a structure map. In the real crystal, interatomic distances are locally elongated or compressed, but if the cross sections and connectivity shown in the lattice image are mapped using the idealized dimensions, the process is directly equivalent to mapping around a Burgers' circuit enclosing the dislocation. A closure gap (or an overlap) will be found between columns that are, in fact, joined in the usual way across a c.s. interface.

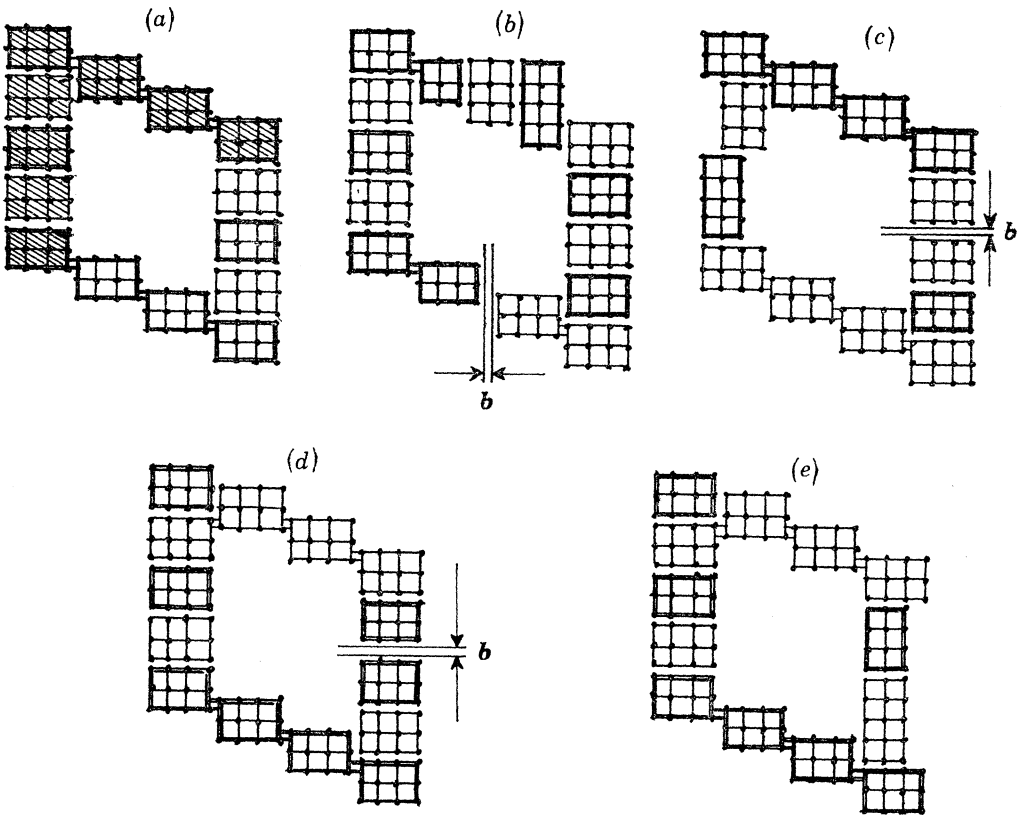

FIGURE 3. (*a*) Perfect $Nb_{12}O_{29}$ structure, showing files of columns (hatched). (*b*) Burgers' circuit round dislocation with $\boldsymbol{b} = \frac{1}{2}a_R[011]$. (*c*) Dislocation, $\boldsymbol{b} = \frac{1}{2}a_R[110]$. (*d*) Dislocation, $\boldsymbol{b} = \frac{1}{2}a_R[110]$. (*e*) Extended defect, related to dislocation (*d*), but with one additional anion row inserted, creating a planar fault.

In figure 3 are schematic Burgers' circuits for dislocations in the $Nb_{12}O_{29}$ structure (figure 3*a*). In figure 3*b*, one additional (001) half-plane of cations has been inserted into the top leg of the circuit, giving $\Delta N = +1$ and a closure gap of $\frac{1}{2}a_R[001]_R$, across which the columns in the bottom leg must be canted. For insertion of an additional half-plane of oxide ions in the left-hand leg of figure 3*c*, $\Delta N = -1$ and the closure gap is $\frac{1}{2}a_R[100]_R$, again requiring that the columns be canted. In both figures 3*d* and 3*e*, three legs of the circuit and the core region are

identical; the top leg is related to 'good' crystal structure by a displacement of $\frac{1}{2}a_R[110]_R$, which produces a displacement of $\frac{1}{2}a_R[100]_R$ in the plane of projection. If, as in figure 3*d*, the original crystal structure is reformed and propagated across the fault, the stoichiometry of the structure is conserved, except in the core, but the layers must be tilted. If, as in figure 3*e*, an additional half-plane of oxygen is inserted, giving $\Delta w = \frac{1}{2}a_R$, $\Delta N = -1$, the strain is eliminated and the cation levels matched up across the c.s. interface. The stoichiometry of the crystal is thereby changed throughout an extended defect of anomalous structure that is propagated through the crystal from its origin in the distorted core. Whereas figure 3*d* represents a pure displacement to which we can assign the Burgers' vector $\boldsymbol{b} = \frac{1}{2}a_R[110]_R$, 3*b* and 3*c* emphasize that the insertion of an extra half-plane of atoms involves the chemistry, as well as the geometry, of dislocations. Because of the close relation between the situations shown in 3*d* and 3*e*, we bring the strain-free extended defects of the latter type into the subsequent analysis of faulted structures. Figure 3 is drawn schematically, but all the faults shown correspond closely to faulted structures that have been observed.

As is shown in figure 3, the closure gap for a Burgers' circuit round a unit dislocation ($\Delta w = 1$) has a component $\frac{1}{2}a_R[010]$; such dislocations are therefore of mixed character. The relation between their screw component and the topology of linked octahedra, as expressed in the changed numbers of columns and c.s. interfaces, merits some consideration. We may define a layer of these structures, with cations at the levels 0, 1, 2... and $\frac{1}{2}$, $\frac{3}{2}$... in terms of a circuit in which changes of level alternate in the regular sequence $0 \rightarrow \frac{1}{2} \rightarrow 0 \rightarrow \frac{1}{2} \rightarrow 0 \rightarrow$ etc. In good crystal, the circuit would close and the sequence would repeat identically. Around a dislocation, because of the change of ± 1 in the number of c.s. interfaces, one circuit would terminate at the original level, but after the incorrect change of level; repetition of the circuit terminates at the original column, but at the level ± 1, after a correct level change. The original discrete layer is thereby wound into a helix with the pitch $\frac{1}{2}a_R$, as expressed by the Burgers' vector. This is the case for displacements $\frac{1}{2}a_R[u\ v\ w]$ with $u+w$ odd. For $u+w$ even, $\Delta N = 0$ or ± 2 and there is no mismatch of cation levels at the closure gap: the dislocations can have pure edge character. In such dislocations, relaxations that shift c.s. interfaces in the region surrounding the core (i.e. operation 1 of table 1) may enable the sub-cell structure to retain complete order, eliminating distortions, even in the core itself, through the formation of columns of unusual cross section.

A pure screw dislocation, parallel to $[010]_R$, would necessarily have the Burgers' vector $\boldsymbol{b} = a_R[010]$, since the operation must bring the octahedral groups into register within each column at the completion of every circuit. Such a screw dislocation, in the orthorhombic $Nb_{12}O_{29}$ structure, is illustrated in figure 4. At each c.s. interface, the cations in the columns B lie $\frac{1}{2}a_R$ below those in columns A, and alternation of levels is preserved round the circuit. In the puckered sheet shown, however, B′ is thus related to layer A′, not to layer A; the oxygen sites X_1 and X_2, Y_1 and Y_2, which would coincide in the undislocated crystal, are

separated by $a_R[010]$. As a consequence of this twisting, interatomic distances immediately around the dislocation line are somewhat elongated and the central core inevitably involves extremely severe distortions in the shape and dimensions of the cation coordination polyhedra.

Lattice image micrographs, at high magnification, seldom provide obvious evidence of distortions, but three effects can be seen in the accompanying plates. Bending of lattice rows around edge dislocations is very subtle, and becomes evident (as in figure 7, plate 1) only through the cumulative effect of successive, closely spaced dislocations. The gradation in dislocation contrast, familiar from low magnification electron microscopy, becomes rather small, but there are recognizable abnormalities in the dark contrast at the c.s. interfaces between

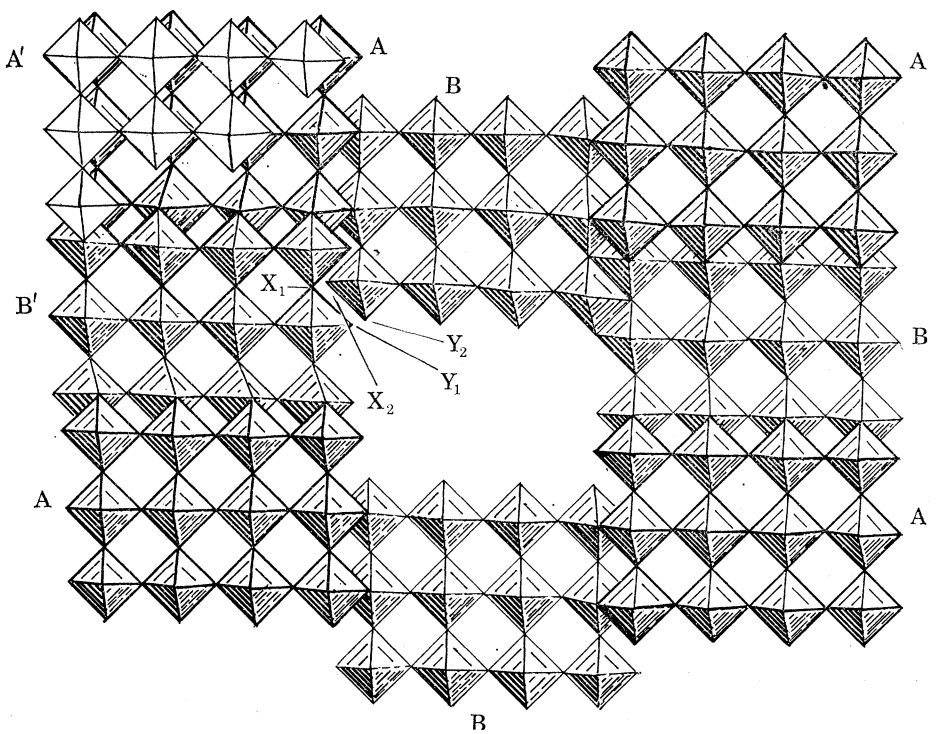

FIGURE 4. Schematic Burgers' circuit round a pure screw dislocation, $\boldsymbol{b} = \frac{1}{2}a_R[010]$.

columns, in and around the dislocated areas, as can be seen in figures 7 and 9, plates 1 and 2. Lattice image contrast is sensitive to small angular deviations between the electron beam and the local normal to the plane of projection, and these abnormalities can be ascribed to the marked buckling of lattice planes when blocks have been canted. All image detail is frequently lost in the dislocation cores. In some cases it can be recognized that the essential structural principles of short range ordering are preserved, even though this results in core columns with unusual

dimensions and cross sections. In other cases, compression or dilation of the substructure apparently results in so great a distortion that irregular displacements of atoms impair any clear projection down the $[010]_R$ axis.

This discussion has been restricted to dislocations parallel to $[010]_R$. A dislocation in any other orientation would impose a drastic reorganization of the whole column structure, layer by layer, down the unique, short crystallographic axis. It is characteristic of these structures – and an essential condition for unambiguous lattice imaging – that crystals retain a high degree of regularity along this unique axis, even although the ordering pattern on identical $(010)_R$ planes is complex. Change of structure from one layer to another would introduce an overlap between their projected structures. 'Overlap contrast' is indeed encountered from time to time and can frequently be understood in terms of occasional jogs in the stacking along $[010]_R$ (Allpress 1972), but the repeated overlap that would arise from an oblique dislocation would obscure all structure in the image of the dislocated region. We have not recognized this effect with certainty and doubt the feasibility of analysing the lattice images that would result from it.

Experimental

Materials

Dislocations and related extended defects were occasionally found in a variety of niobium oxides and related compounds, prepared for other purposes and discussed elsewhere (see, for example, Hutchison & Anderson 1972; Anderson, Browne & Hutchison 1972*b*). Those analysed below were found in studies of the metastable *N*-modification of Nb_2O_5 in the presence of fluoride ion as dopant, of the MgF_2–Nb_2O_5 system (Lincoln, Hutchison & Anderson 1974; Hutchison, Lincoln & Anderson 1974) and of the supposed *M*-modification of Nb_2O_5 (Schäfer, Gruehn & Schulte 1966).

The micrographs discussed here were taken with a JEM 100U electron microscope, at about $\times 300\,000$ magnification, using a high resolution goniometer stage. Specimen crystals were crushed and dispersed on carbon films; flakes of suitable thinness were sought and oriented so that [010] was exactly parallel to the electron beam. A 40 μm objective aperture was used to transmit all diffracted beams out to a reciprocal lattice spacing of approximately 2.5 nm^{-1}, and micrographs were recorded in through-focus series bracketing the Scherzer optimum defocus condition (about -90 nm with the optics used). As is now well established (Cowley & Iijima 1972; Allpress & Sanders 1973), under these conditions and for a sufficiently thin crystal (not exceeding 10–15 nm), the lattice image contrast approximates to the projected charge density of the crystal and can be directly interpreted in terms of the structure. The resolution attainable with the JEM 100U was insufficient to resolve the cation positions within the ReO_3 structure of the individual columns, but the close spacing of cation rows at the c.s. interfaces delineates each column in a framework of dark contrast. Measurement of the columns, so outlined,

enables their cross sections to be identified without ambiguity. Their connectivity can be assigned from the relative positions of adjacent columns: cation rows are continuous (at 0.4 nm spacing) across a c.s. interface, but are displaced by 0.2 nm between columns linked at the same cation level, as may be seen from figure 1. Although the projected charge density approximation breaks down in thicker crystals, as a result of dynamical effects, it was usually possible to trace the outlines, dimensions and spatial relations of the columns into the rather thicker portions of wedge shaped flakes. By these methods, exemplified in the other papers cited, the structure around dislocations and boundaries could be mapped and drawn out in idealized form, in terms of the octahedron diagonal as module.

Experimental results

A number of lattice images containing evidence of dislocations and related defects has been examined in detail, and the analysis of four of these, representing different types, is presented. The first of these – the generation of a domain of twinned structure, on a permitted twinning plane, by the insertion of a wedge of transformed structure – may perhaps not strictly involve a dislocation process. It is included because it can be formally represented by a displacement operation and clearly exemplifies the rules set out earlier; it generates a closed domain of anomalous structure and, although the cations occupy sites compatible with the architecture of the block structures, it is likely that small residual strains remain. By 'permitted' twinning is implied the twinning of a structure across a habit plane that preserves both the full coherence and the stoichiometry of the structure; in general, these requirements impose severe restrictions on the modes of twinning that are possible. However, crystals are occasionally found that are twinned on 'forbidden' orientations, which necessarily involve a boundary that is not fully coherent, is likely to involve a dislocation array and that imposes locally a departure from the proper stoichiometry. Similarly, the semi-coherent intergrowth of two block structures requires the formation of one boundary presenting an array of dislocations, which might be regarded as transformation dislocations. Although the structures differ on either side of the semi-coherent boundary, both are superstructures of the same ReO_3 type sub-cell, and it may be noted that the Burgers' circuit is defined in terms of that sub-cell.

Incoherent twinning in ribbon structures

By 'ribbon' structures we denote those such as $Nb_{12}O_{29}$ (figure 1) or N–Nb_2O_5 (figure 5; $Nb_{16}O_{40}$, structure symbol denoting column cross section and linkage of columns at the same level $(4 \times 4)_\infty$), in which the ReO_3-like columns are joined in infinite strings by sharing octahedron edges between contiguous columns with cations at the same level. For ribbon structures, planes parallel to $(100)_R$ and $(001)_R$ of the sub-cell are permitted twin planes, and a twinning operation of that kind in N–Nb_2O_5 is seen in figure 5, plate 1. At B and B′ the ribbon direction is

reversed as a result of twinning initiated at a point within a horizontal file of (4×4) columns. This opens out a wedge of anomalous column configurations which, at C and C′, has widened enough to accommodate exactly an integral number of (4×4) columns. At these points the crystal could resume the growth of undistorted structure. The structure between files B and C, as mapped from the micrograph, is shown in figure 6.

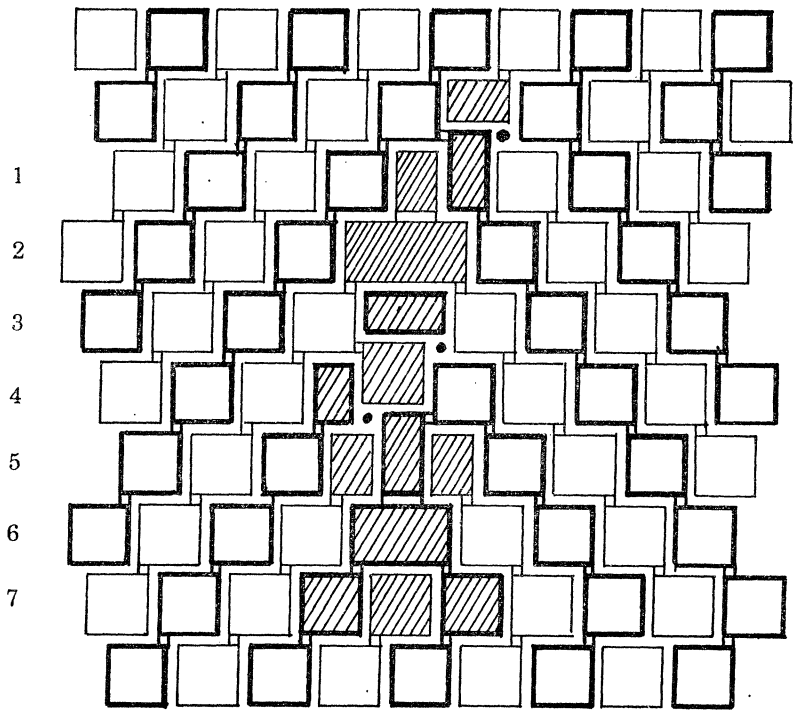

FIGURE 6. Structure, mapped from the area enclosed in the rectangle in figure 5. Hatched columns shower 'filler' wedge; its structure conforms to table 1.

This twinning can be formally described as produced by the operation of a displacement vector $\boldsymbol{b} = \frac{1}{2}a_{\mathrm{R}}[310]$ on the normal structure at B and at each of the next six files of columns. At D (figure 5), the same displacement vector operated once only, and was reversed after three files of columns. At each operation, three additional atom rows are inserted into the crystal and the situation is exactly analogous to that of figure 3*e*. In both the inserted wedges BC, B′C′, 2 cation rows $+1$ oxygen-only row have been added at each of the steps 1, 3, 4, 5 and 7; 1 cation row $+2$ oxygen rows at steps 2 and 6. The total insertion of 12 cation rows $+9$ oxygen rows makes up three complete (4×4) columns to complete the wedge. At each step, the numbers and the cross sections of columns are adjusted, in conformity with the relations established above; the inserted structure involves no major distortions but does impose some abnormal column cross sections. Essentially the

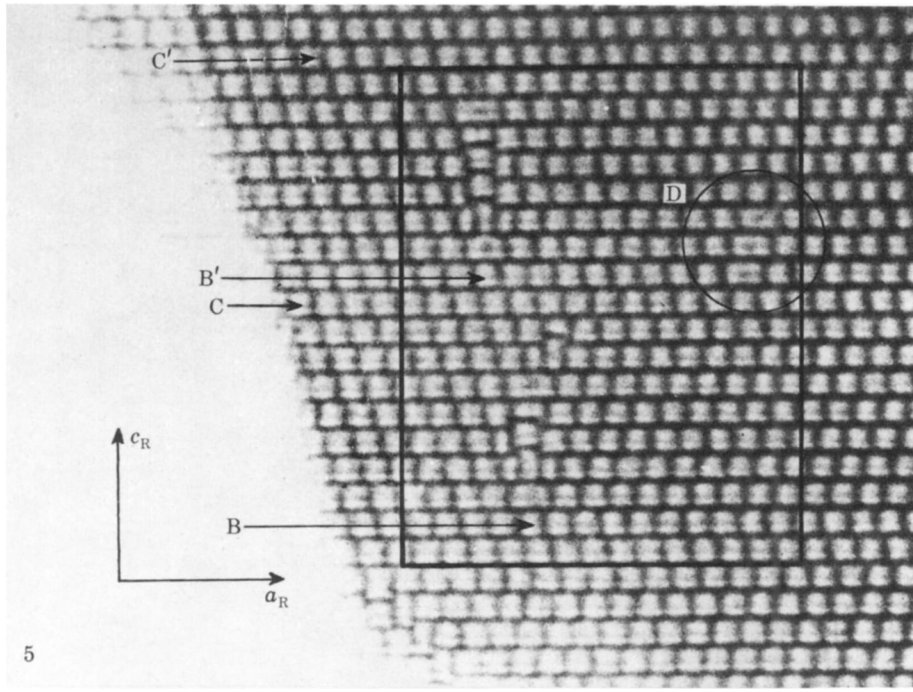

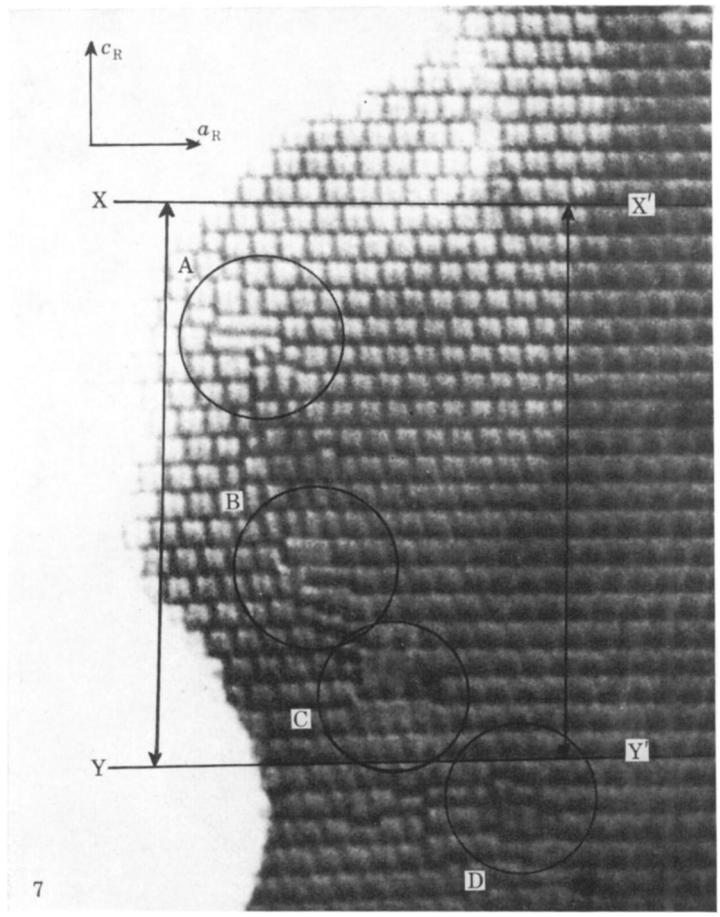

FIGURE 5. Internal twinning in N–Nb_2O_5.

FIGURE 7. Series of dislocations in N–Nb_2O_5.

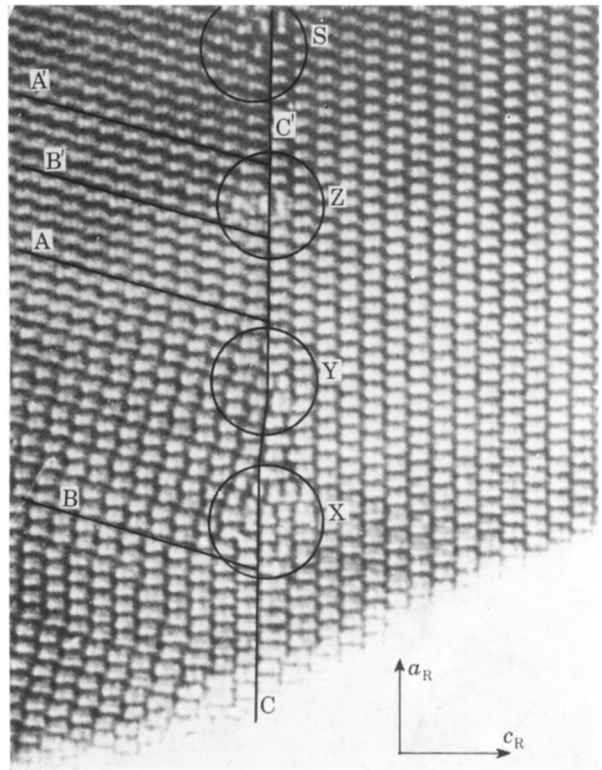

FIGURE 9. Intergrowth of the $Nb_{12}O_{29}$ and $Nb_{25}O_{62}$ type structures: coherent on (100) ($Nb_{12}O_{29}$); incoherent along the boundary C–C′.

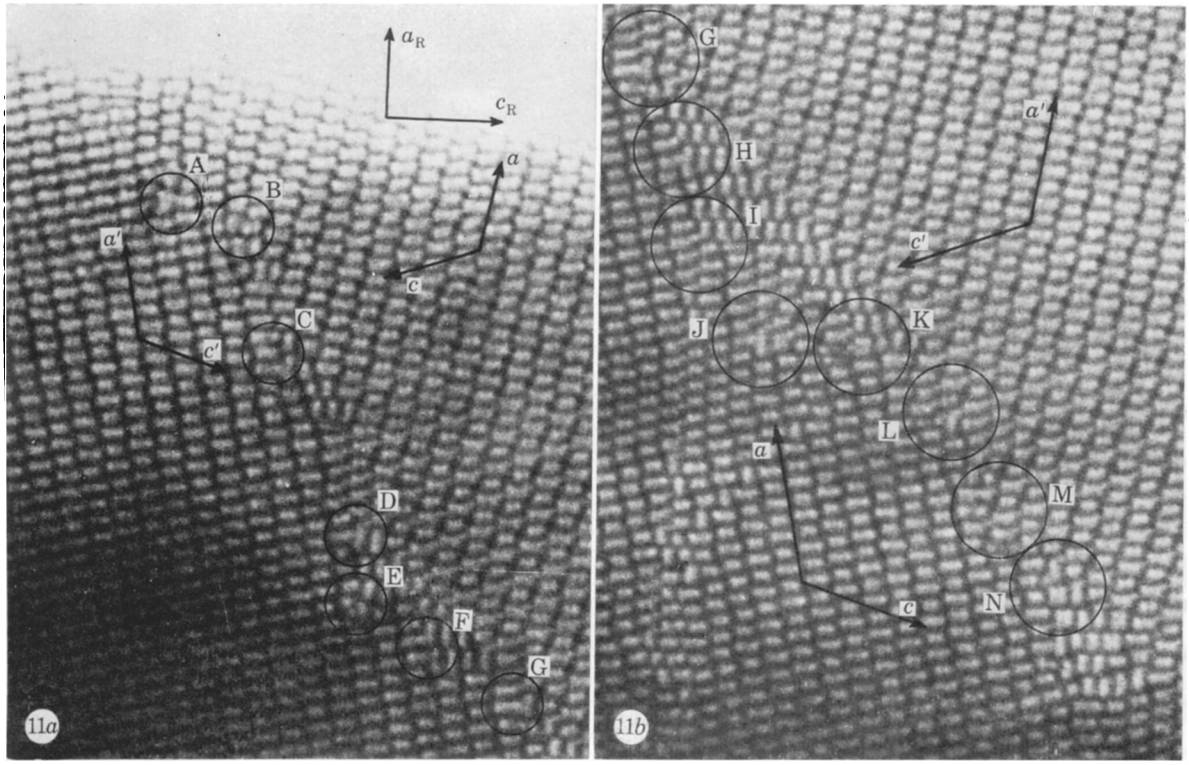

FIGURE 11. Forbidden twinning on $(001)_R$ in H–Nb_2O_5, with successive dislocations at the boundary. The field (*b*) overlaps that of (*a*) at dislocation core G.

same structure is found in both the dislocations and each core necessarily contains a column of T-shaped cross section, with an unusual mode of octahedron edge-sharing. If it can be assumed that the structure is substantially free from point defects, the local composition is implicit in the column configuration adopted. On this basis, the anion:cation ratio in each core is about 2.514: since an over-all charge balance must be preserved, the probable implication is that impurity atoms (cations with formal charge > 5, or singly charged anions such as F′, OH′) are concentrated in the core. As compared with the host structure, rows 1, 4 and 5 appear to be anion-deficient, rows 2, 3 and 6 cation deficient. Unless these local compositions are fully compensated by impurity atoms and point defects, it is likely that the structural pattern imposed by the geometry of the extended defect brings with it a considerable degree of charge separation.

Analogous twinning dislocation systems have been analysed in other structures (e.g. in the $(5\times 3)_\infty$ structure of $MgNb_{14}O_{35}F_2$). For columns three octahedra in width, the operative displacement vector is $\frac{1}{2}a_R[110]$, and one atom row is added at each step. Alternate insertion of cation rows and oxygen rows in five successive steps can complete the core of an extended defect, by generating one complete additional column of standard size.

Arrays of edge dislocations in N–Nb_2O_5

Figure 7, plate 1 shows a succession of edge dislocations in N–Nb_2O_5, lying along a meandering line and continuing into the thicker part of the crystal flake where the structure is poorly resolved. In the immediate neighbourhood of this line, the contrast at the column interfaces is distinctly abnormal and the structure is perturbed by the insertion of columns with the 'wrong' cross section; away from the – in some cases very ill resolved – dislocation cores, the crystal structure is good. The cumulative effect of this dislocation array is a substantial degree of elastic strain. Assigning idealized dimensions, and measuring between points, in good crystal, that lie on the same lattice row, the distance X–Y on the left hand side of the crystal should be 28.6 nm; on the right side, the distance X′–Y′ should be 28.0 nm. In effect, three additional lattice rows have been inserted at the left between the two files of columns X–Y′ and Y–Y′. In joining up around this distortion, the [001] planes – seen as the c.s. planes running horizontally between the files of columns – are discernibly bent, by about 2°, in the immediate proximity of the dislocation C.

An analysis has been made of the four dislocations marked in figure 7. In A (figure 8), the upper part of the core shows two very elongated columns, each arising from the elimination of two c.s. interfaces and so replacing three columns of the host structure; these arise from the operation of a dipole of types (3) and (4) (table 1), eliminating one cation row and inserting one oxygen row, both running in the vertical direction. Immediately below this, the distortions are too great for interpretation of the core structure, but application of the rules summarized in table 1 shows that a vertical cation row is eliminated and an additional horizontal

cation row inserted at that place, giving a net displacement vector $\boldsymbol{b} = \frac{1}{2}a_{\mathrm{R}}[10\bar{1}]$. The composition of this core region is about $NbO_{2.496}$. In dislocation B the core region can be analysed with some confidence. There is again an elimination of column interfaces and formation of elongated columns as a (vertical) cation row is replaced by an oxygen row. At the left side of the core, a pair of columns is spliced or overlapped to form a diagonal tunnel configuration (Hutchison &

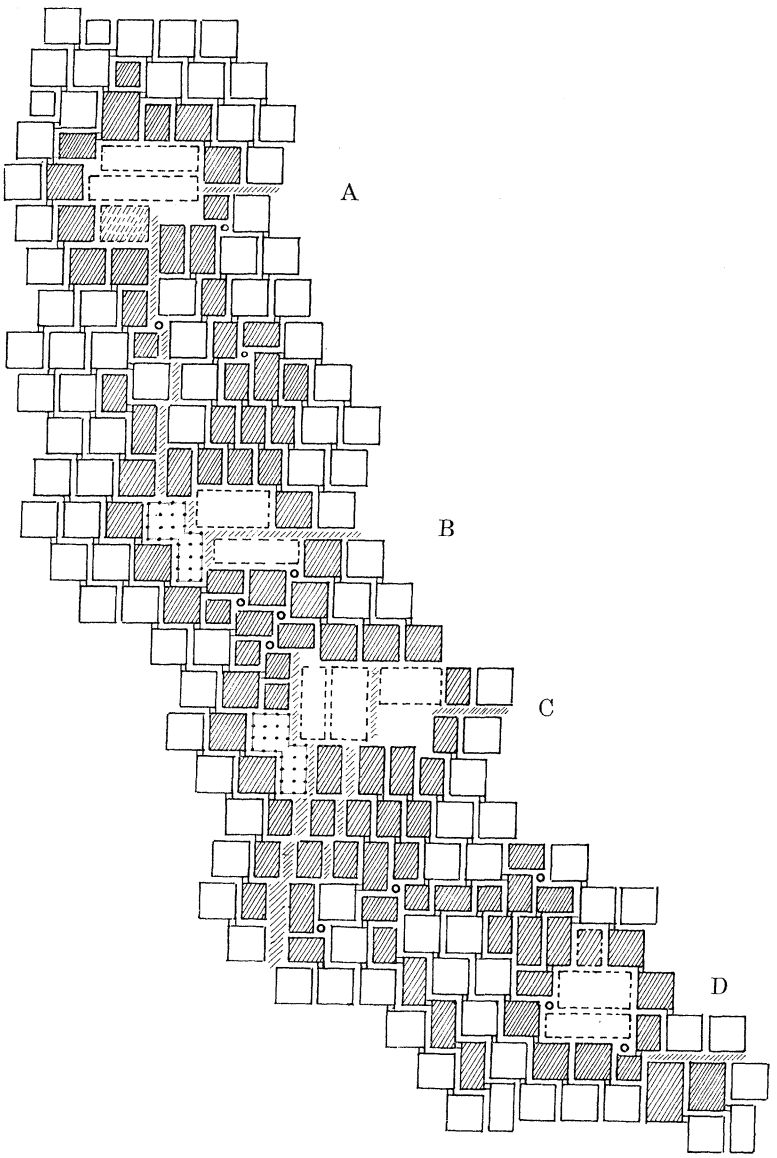

FIGURE 8. Structure around dislocations A, B, C, D of figure 7. Hatched columns show extent of structural reorganization around the cores.

Lincoln 1973) and to introduce an extra oxygen row at the left side. The net displacement is $\frac{1}{2}a_R[101]$ and the composition of the core is about $NbO_{2.496}$.

The cumulative distortion resulting from these dislocations (evident in the micrograph), together with the increasing thickness of the crystal flake, makes analysis of dislocation C less certain, but it is probably as shown in the figure. Across the six files of columns that enclose the core, the net effect is to insert one additional horizontal cation row at the left and to eliminate one vertical oxygen row at the lower boundary, giving a net displacement of $\frac{1}{2}a_R[10\bar{1}]$. In the core itself, however, the observed sizes and positions of the columns cannot be mapped without assuming that both a cation row and an oxygen row have been eliminated over a length of about 4 nm – a dipole, separating the partials but with the over-all effect of operation 2, table 1 – leaving a highly dilated region, with stretched interatomic distances. The composition of the core region is again close to $NbO_{2.497}$. The total effect of A, B and C is to give the discrepancy in dimensions between right hand and left hand halves of the crystal, referred to above.

Dislocation D, which abuts closely upon C, involves a large region of severe distortion and there are some uncertainties in mapping it. Abnormal image contrast may be associated with dilation of the structure in rows I and II, immediately below core C. A vertical cation row terminates at row V and an oxygen row at row VII, adding an additional 0.4 nm to the strain that must be accommodated. In addition, an extra horizontal cation row is inserted on the left, at row VII. The total displacement is $\frac{1}{2}a_R[211]$ and the (010) lattice planes must be buckled to allow for the mismatch of cation levels round the dislocation. The composition of the core is close to $NbO_{2.500}$.

This array of dislocations has no defined crystallographic orientation but distorts the crystal so that, below dislocation B, it could be regarded as a low angle tilt boundary between two segments misaligned by about 2°. Dislocations recur along it at spacings of about 6 nm. Each core has a central region about 4–5 nm in diameter, with a highly anomalous structure that yet conforms, as far as possible, to the topology of linked octahedral NbO_6 groups. Surrounding this is a roughly elliptical region within which column sizes are reorganized, with its longer axis roughly parallel to $[10\bar{1}]$ of the sub-cell. In each case, the total composition of the core is close to that of the matrix crystal; formation of the reorganized structure does not appear to depend upon the availability and segregation of ions of different charge state and it may be inferred that the cores are essentially built up from Nb^{5+} and O^{2-}. Within this over-all material balance, however, it is noticeable that the principle of local electrostatic neutrality is breached. In each case, the central, most distorted region of the core contains columns that, from their cross-section, must be hyperstoichiometric: the peripheral region has columns that are substoichiometric with respect to the matrix material. This implies a significant degree of charge separation, with a net anionic charge residing in the central core region, surrounded by a ring bearing a net cationic charge.

Semi-coherent intergrowth dislocations

It is implicit in the crystal chemistry of the niobium oxide structures that two distinct structures, differing in chemical composition, may be able to form perfectly coherent intergrowths. This can happen if one or other of the two sets of c.s. planes that demarcate the ReO_3-like columns is common to both structures; such a c.s. plane provides a coherence plane. Thus the [001] planes of the $Nb_{25}O_{62}$ and the $Nb_{12}O_{29}$ structure types are identical in their stepped configuration, and intergrowth is possible across this interface, as shown in figure 9, plate 2.

As long as the lamella of intergrown structure runs right across a crystal, there is no distortion or misfit. However, because the superstructure feature that differentiates column structures is the operation of different *pairs* of c.s. planes, it is not possible, in general, to find more than one coherence plane for any pair of compounds: except in certain special cases, coherent intergrowth in two directions is forbidden. In the course of our work it has been found that inception of coherent intergrowth occasionally takes place in the middle of a file of columns defining the habit plane. This is particularly the case when, as in the system $Nb_2O_5 + MgF_2$ (Lincoln *et al.* 1974), the phase equilibria are complex. Figure 9 shows a crystal of $Mg_2Nb_{10}O_{25}F_4$ ($Nb_{12}O_{29}$ type $(4\times3)_\infty$). On the left side, between the lines A–B, A′–B′ are lamellae of $MgNb_{24}O_{60}F_2$ ($Nb_{25}O_{62}$ type $(4\times3)_2$) in coherent intergrowth along [001], but terminating within the crystal and so necessarily meeting the matrix structure along a boundary C–C′. The two structures cannot match their configurations along this direction without local modification of structure and introducing distortions. A semi-coherent boundary is created by changing the column sizes and introducing a succession of dislocations, at intervals of 8–10 nm, with a displacement of $\frac{1}{2}a_R[110]$ at each dislocation, corresponding to the insertion or deletion of one lattice row.

A corresponding Burgers' circuit enclosing three dislocations is shown in figure 10. Proceeding upwards, one oxygen row is removed at X, a core involving two columns of anomalous cross section. At Y, a cation row is removed. At Z another oxygen row is removed. Between X and Y, and from Z upwards, the total projected displacement vector is odd and lattice planes must be warped to adjust the cation levels at the column interfaces. That anomalies in resolution and contrast are more pronounced at X and Z may perhaps be associated with the greater reorganization of column structure and consequential distortions at these dislocations, as compared with Y. Between Y and Z the displacement is $a_R[100]$; there is no mismatch of levels, and expansion of the structure can be accommodated by distortion-free adjustment of column sizes.

The nature of this extended defect is such that the crystal is chemically inhomogeneous; the anion:cation ratio of the host is 2.417, that of the intergrowth 2.480. Compositions of the dislocation cores, averaged over a circle of about 3 nm radius, are 2.443, 2.449 and 2.447 for X, Y and Z respectively – they represent averaged boundary material.

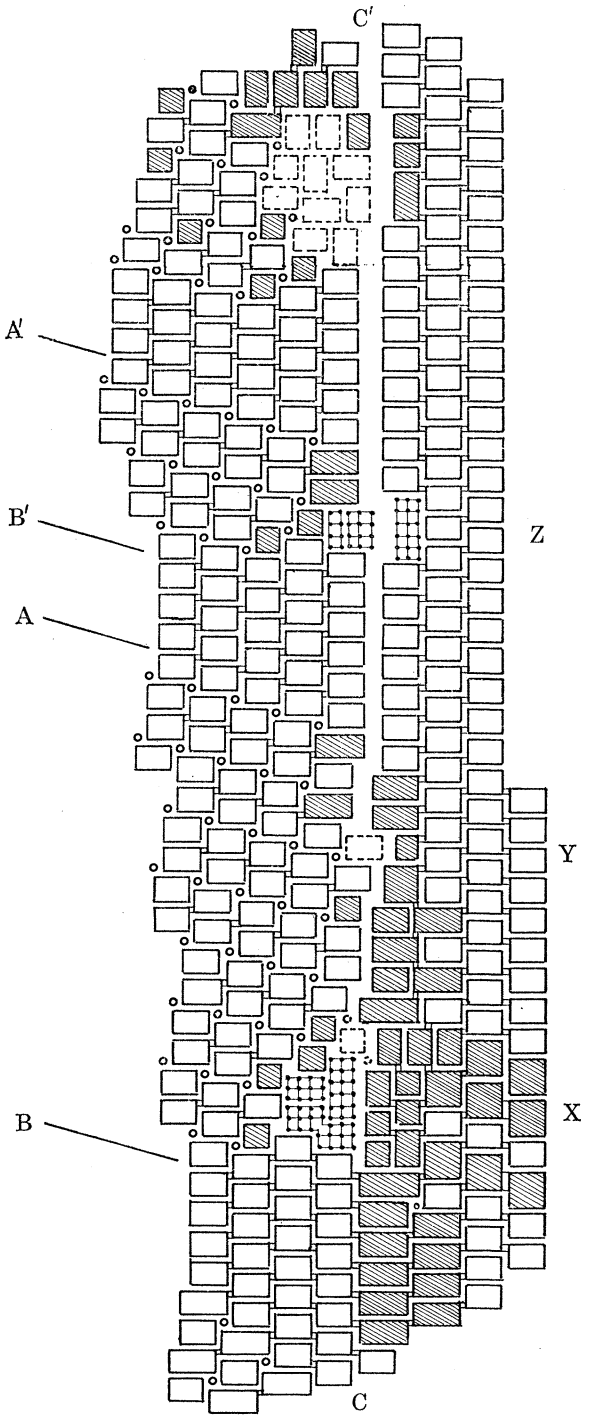

FIGURE 10. Structure around the boundary C–C′ of figure 9. Successive dislocations with $\boldsymbol{b} = \frac{1}{2}a_R[011]$ at X, Y, Z. Hatched columns show reorganized structure.

At S, about 10 nm above Z, is another localized area of abnormal image contrast, suggestive of another dislocation core. Careful analysis of this region reveals no dimensional mismatch in the plane of projection and no alterations in the numbers of cation rows and anion rows. There is, however, the change of contrast, loss of resolution and reorganization of column dimensions associated with known dislocations. It seems probable that this can be interpreted as a pure screw dislocation which, as has been seen, produces no dimensional anomalies when viewed in [010] projection. Our observations suggest that pure screw dislocations are rare.

Forbidden twin boundaries

Strict constraints on twinning in niobium oxide structures have already been indicated. Not only must possible composition planes lie parallel to the symmetry planes of the cubic sub-cell; there is the further restriction that the complete column is the structural unit that must be reflected across the mirror plane. As a consequence, not all structures can twin at all. In the case of H–Nb_2O_5, the only permitted twinning is across $(10\bar{1})$, which is also the $(10\bar{1})_R$ plane of the sub-cell (Anderson *et al.* 1972*b*). However, crystals of disordered H–Nb_2O_5 have been found from time to time, which give streaked electron diffraction patterns that closely resemble the diffraction pattern that has been assigned to the supposed *M* polymorph of Nb_2O_5 (Mertin, Andersson & Gruehn 1970). These streaked patterns can, however, be indexed in terms of intergrowths between domains of H–Nb_2O_5 structure that are related by reflection across the forbidden $(100)_R$ plane, and this interpretation accords with the lattice images from such crystals.

No fully coherent boundary can be formed between domains related in that way. The one set of columns, forming the extended ribbons of (5×3) columns, could indeed be folded as required, but the other set, of isolated (4×3) columns cannot be so treated. A drastic rearrangement of column cross sections and a change in local stoichiometry is unavoidable. The boundary between forbidden twin domains has only once been found, and is shown in figure 11, plate 2, at rather low resolution (probably about 0.6 nm). In the crystal, the ReO_3 sub-cell axial directions remain unchanged across the whole field of the micrograph; the left hand and right hand halves consist of good H–Nb_2O_5 structure, but with their axial directions in a mirror image relation. The junction between the domains forms a band, roughly 5 nm wide, running in a crystallographically indeterminate direction, within which column dimensions are substantially rearranged. There is a succession of dislocation cores, spaced about 5–6 nm apart. Although the resolution of the micrograph is poor, it has been possible to analyse several of these, although the distortion in the core regions is in several cases too great for detailed, reliable interpretation.

The structure of the semi-coherent boundary, spanning ten consecutive dislocations, is shown in figure 12. Only at one place, in dislocation D, can a simple folding of the (5×3) ribbons be observed. Elsewhere, the extensive reorganization of column sizes and interfaces obscures the relative displacements needed for transition between the two domains. These displacements are not produced by a

succession of simple edge dislocations, but predominantly take the form of dipoles replacing a cation row by an oxide ion row, without change in over-all dimensions; this substitution is effected within some unusual column configuration in the core. As already indicated, this row substitution can be treated as the sum of dislocations of opposite sense, acting on the cation rows and oxygen rows respectively, on either side of a common glide plane. In dislocation I, these partials appear to terminate about 3 nm apart, leaving the core highly dilated; in dislocation E they overlap, creating an overcrowded core region. Over much of this semi-coherent boundary, the structure adopted is compatible with the dimensions of normal apex- and edge-sharing between octahedral groups, and can be mapped in projection in terms of conventional columns. However, the lattice image suggests a degree of distortion in the core material that is not fully explained if the core and its surroundings are dimensionally matched. This distortion would be accounted for if there were a screw component in the dislocations, but that supposition cannot be tested experimentally.

The structure along the line of dislocations implies a considerable local change

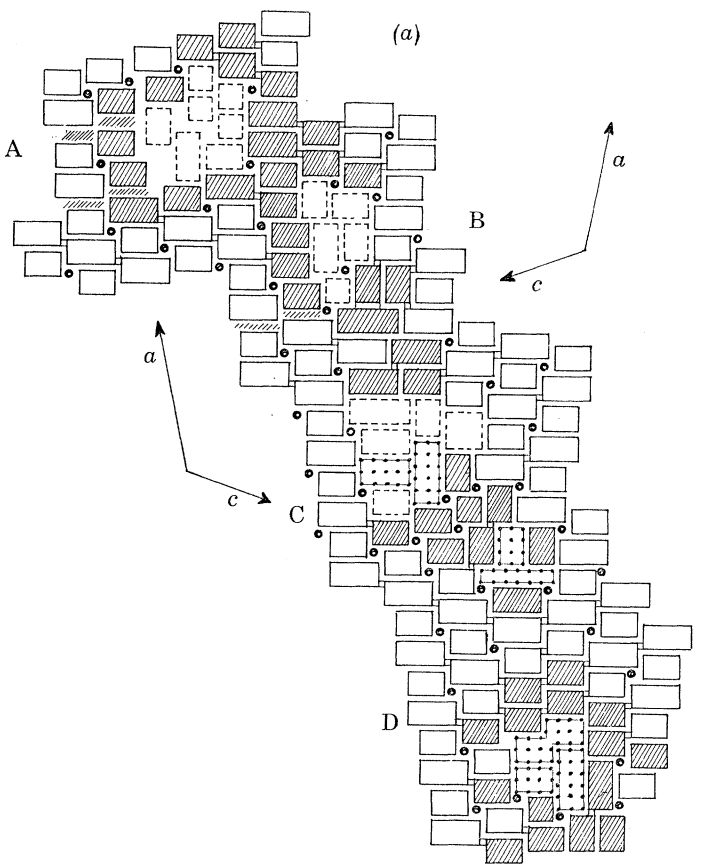

FIGURE 12. For description see opposite.

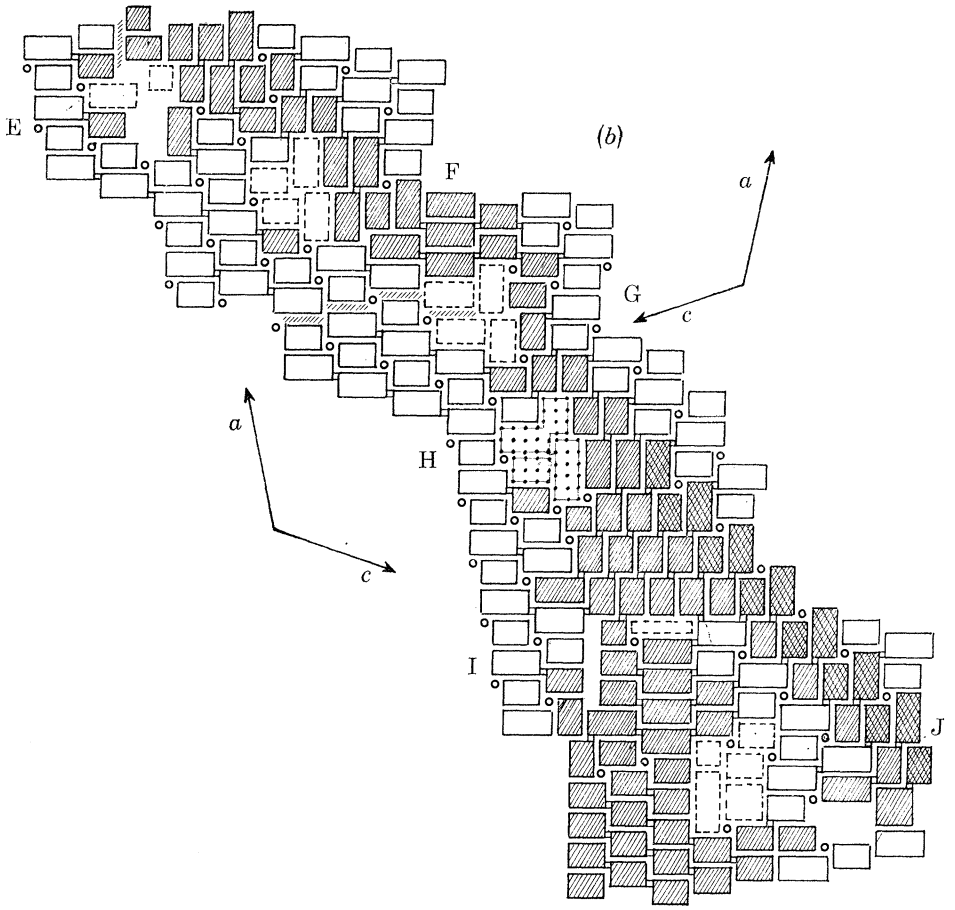

FIGURE 12. Structure of dislocated forbidden twin boundary in figure 11.
(*a*) Dislocations A–D; (*b*) dislocations E–J.

in stoichiometry, with an average composition about $NbO_{2.48}$. Since the material showed no evidence for reduction of the niobium, it is likely that impurity cations, of lower valency, had been concentrated and segregated into the boundary.

CONCLUSION

The foregoing discussion of the fine structure of dislocations is capable of extension to other types of crystal structures that can be treated topologically in terms of the linkage of polyhedra. We have recently found, and analysed the microstructure of, dislocations in another octahedron structure – the perovskite-related compounds $(Bi_2O_2)Ba_{n-1}Ti_nO_{3n+1}$ (Hutchison, Anderson & Rao 1975). In these also, the local structure and ordering within the core regions of large edge dislocations is adjusted in unit steps consistent with the topology. Subject to the inherent differences between octahedron networks and tetrahedron networks, similar considerations apply to the structure and chemistry of dislocations and

related planar defects in silicate structures (see Chisholm 1975; Hutchison & McLaren, to be published). Thus our analysis provides a useful tool for relating the evidence of lattice imaging microscopy to perturbed local structure in crystals, and has been applied not only to grown-in dislocations, such as are exemplified here, but also to the study of precursor stages in solid state reactions (Browne & Anderson 1974; Obayashi & Anderson, to be published).

It does not appear profitable to attempt to extract quantitative estimates of dislocation energies from the results. What has been established is that there may be discrete and far reaching local rearrangements of structure in the core region, superimposed upon the more subtle relaxations of atomic positions that can be treated by elastic theory. There is both a lattice energy component and a strain component. In polyhedron structures, the latter can be considered, qualitatively at least, as involving distortion of metal–oxygen–metal bonds, and it should be related to the vibrational spectrum of the crystals; we have recently analysed the infrared and Raman spectra of the crystalline niobium oxide structures. Compressive strain could be accommodated by a twisting of the octahedral groups, to shorten the metal–metal distances, and the strain energy should be related to the force constant for the metal–oxygen–metal local bending modes. Tensile strain will be similarly related to the symmetrical stretching mode. The spectroscopic evidence is that the latter has the larger force constant. It is certainly true that deformation is more extensive on the compressed side around an edge dislocation in the Aurivillius perovskite-related structures; in the niobium oxides, discussed here, the evidence is inconclusive.

The authors would thank the Science Research Council for its continued support of this work.

References

Allpress, J. G. 1972 *J. Solid State Chem.* **2**, 78.
Allpress, J. G. & Iijima, S. 1973 *J. Solid State Chem.* **7**, 89.
Allpress, J. G. & Sanders, J. V. 1973 *J. appl. Crystallogr.* **6**, 165.
Anderson, J. S., Browne, J. M. & Hutchison, J. L. 1972*a* *Nature, Lond.* **237**, 155.
Anderson, J. S., Browne, J. M. & Hutchison, J. L. 1972*b*. *J. Solid State Chem.* **5**, 419.
Browne, J. M. & Anderson, J. S. 1974 *Proc. R. Soc. Lond.* A **339**, 463.
Chisholm, J. E. 1975 *Surface and defect properties of solids*, vol. 4, 126. London: The Chemical Society.
Cowley, J. M. & Iijima, S. 1972 *Z. Naturforsch.* **27**a, 445.
Hutchison, J. L. & Anderson, J. S. 1972 *Phys. Stat. Solidi* (*a*) **9**, 207.
Hutchison, J. L., Anderson, J. S. & Rao, C. N. R. 1975 *Nature, Lond.* **255**, 541.
Hutchison, J. L. & Lincoln, F. J. 1973 *Phys. Stat. Solidi* (*a*) **17**, 169.
Hutchison, J. L., Lincoln, F. J. & Anderson, J. S. 1974 *J. Solid State Chem.* **10**, 312.
Iijima, S. 1971 *J. appl. Phys.* **42**, 5891.
Iijima, S. 1973 *Acta Crystallogr.* A **29**, 18.
Lincoln, F. J., Hutchison, J. L. & Anderson, J. S. 1974 *J. Chem. Soc., Dalton Trans.* 115.
Mertin, W., Andersson, S. & Gruehn, R. 1970 *J. Solid State Chem.* **1**, 419.
Schäfer, H., Gruehn, R. & Schulte, F. 1966 *Angew. Chem.* **78**, 28.
Wadsley, A. D. & Andersson, S. 1970 *Perspectives in structural chemistry* (eds J. Dunitz & J. A. Ibers). New York: Wiley.